Korean J. of Chem. Eng., **6**(3) (1989) *227-233*

BOUNDARY-LAYER ANALYSIS OF POWER-LAW FLUIDS

Byung Kyu KIM and Hak Sung LEE*

Dept. of Polymer Science and Engineering, Pusan National University, Pusan 609-735, Korea
*Dept. of Chemical Engineering, University of Ulsan, Ulsan 680-745, Korea
(Received 19 November 1988 • accepted 27 March 1989)

Abstract—An exact numerical solution to the 2-D(Two-Dimensional) laminar boundary-layer equations of power-law non-newtonian fluids is obtained using a finite difference technique. No limitation has been imposed on the flow behavior index(n) or generalized Prandtl number. As a test case, velocity and temperature fields around a circular cylinder in crossflow were calculated. The result clearly indicated that heat transfer of power-law materials is governed by shear dependent viscosity.

INTRODUCTION

Recently, non-Newtonian fluids such as molten plastics, slurries, polymeric solutions etc. have widely been encountered in many chemical industries. The basic transport behavior of these fluids has therefore been a popular topic for both theoretical and experimental investigators. These non-Newtonian fluids are in essence viscoelastic when in motion, and generally a comprehensive constitutive equation should be sought to relate the local stress to the hydrodynamic variables of the system. However, for certain class of non-Newtonian fluids such as CMC (Carboxyl Methyl Cellulose) solution and paste, a purely viscous model can describe the rheological behavior very closely. A two-parameter model, i.e., power-law model will be considered in this paper.

The internal flow problems of various non-Newtonian fluids have in the past been primarily studied due to the relative importance and simplicity of the flows in ducts and channels. The external flow problems of non-Newtonian fluids are also of much interest in the design of a number of industrial applications including the designs of heat exchanger and many separation process units. Laminar boundary-layer flows of non-Newtonian fluids are presently amenable to theoretical analysis under conditions where the fluid behaviors follow the power-law model.

As far as the boundary-layer flows are considered, the well-known laminar boundary-layer equations were first extended to include power-low fluids by Acrivos and his coworks in early 1960's [1-3]. A generalized Reynolds number and a generalized Prandtl number were properly recognized and discussed. The boundary-layer equations are nonlinear and thermal energy equation is coupled with the velocity. Methods of solution to the momentum equation included Karman-Pohlhausen integral method [1,4], asymptotic expansion [2], Blausius series expansion [5] etc. and these are reviewed in ref. (5). The solution to the thermal energy equation included an asymptotic expansion for large Prandtl number [3], and a series expansion [5]. However, the above solutions were either limited to analytical approximations or valid for a narrow range of power-law materials, and sometimes the predicted heat transfer rates were opposite even in tendency. Certainly, the solutions to the power-law boundary-layer equations are limited, and a very limited number of heat transfer experiments also pose a difficulty for comparison [3,6].

The purpose of this paper is therefore to provide an exact numerical solution to the 2-D laminar boundary-layer equations of power-law non-Newtonian fluids. As a test case, heat transfer from a circular cylinder in crossflow has been chosen. The attached flow velocity and temperature (or concentration) profiles were calculated for a wide range of flow behavior index (n) and generalized Prandtl number. A Göetler-type variable was introduced and a finite difference scheme was implemented on computer in this variable domain. The method of finite difference today may be a simple exercise. However, to the knowledge of present author no one has attempted to solve the problem by this method, and it should be more reliable than any other analytical approximations.

MATHEMATICAL MODELING

Two-dimensional laminar boundary-layer equations of power-law fluids are formulated in this section.

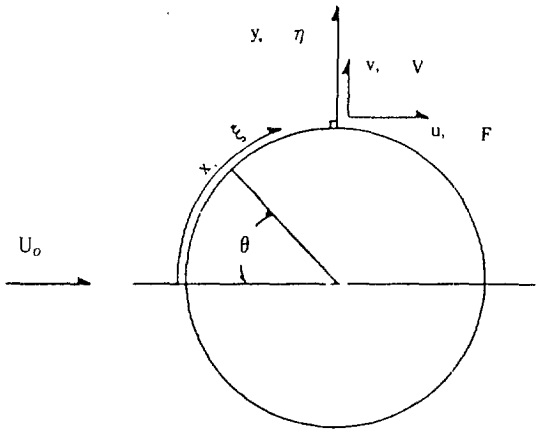

Fig. 1. Boundary-layer coordinate.

The Newtonian counterparts of the governing equations are easily obtained by simply letting the flow behavior index (n) equal to one in the generalized equations. A forced convection with no viscous dissipation has been assumed. The mass transfer problem is limited to convective transport of a non-reacting binary system of dilute solution.

1. Dimensional form of the governing equations

The dimensional form of the governing equations (see coordinate system in Fig. 1) read

$$\frac{\partial u}{\partial x}+\frac{\partial v}{\partial y}=0 \tag{1}$$

$$u\frac{\partial u}{\partial x}+v\frac{\partial u}{\partial y}=-\frac{1}{\rho}\frac{\partial p}{\partial x}+\frac{1}{\rho}\left(\frac{\partial \tau_{xx}}{\partial x}+\frac{\partial \tau_{yx}}{\partial y}\right) \tag{2}$$

$$u\frac{\partial v}{\partial x}+v\frac{\partial v}{\partial y}=-\frac{1}{\rho}\frac{\partial p}{\partial y}+\frac{1}{\rho}\left(\frac{\partial \tau_{xy}}{\partial x}+\frac{\partial \tau_{yy}}{\partial y}\right) \tag{3}$$

$$u\frac{\partial T}{\partial x}+v\frac{\partial T}{\partial y}=\alpha\left(\frac{\partial^2 T}{\partial x^2}+\frac{\partial^2 T}{\partial y^2}\right) \tag{4}$$

$$u\frac{\partial C}{\partial x}+v\frac{\partial C}{\partial y}=D\left(\frac{\partial^2 C}{\partial x^2}+\frac{\partial^2 C}{\partial y^2}\right) \tag{5}$$

The boundary conditions imposed are

$$u(x,0)=v(x,0)=0 \tag{6}$$

$$u(x,\infty)=U_e(x) \tag{7}$$

$$T(x,0)=T_w \tag{8}$$

$$T(x,\infty)=T_e \tag{9}$$

$$C(x,0)=C_w \tag{10}$$

$$C(x,\infty)=C_e \tag{11}$$

In the above equations, subscripts w and e denote the applied conditions at the wall and at the edge of boundary layer, respectively.

For Newtonian fluids it is postulated that the stress tensor is directly proportional to the deformation tensor, and viscosity is a pure physical property. For power-law fluids, however, the viscosity is a function of the second invariant of the deformation tensor leading to a constitutive equation of the form

$$\underline{\tau}=\eta\underline{\dot{\gamma}}, \tag{12}$$

where

$$\eta=m|\dot{\gamma}|^{n-1} \tag{13}$$

in which m (NS^n/m^2) is a constant and the magnitude of deformation tensor is easily approximated as

$$|\dot{\gamma}|=\left|\frac{\partial u}{\partial y}\right| \tag{14}$$

2. Boundary-layer approximation

The above two equations (eqs. 2 and 3) are highly nonlinear. Useful solutions can be obtained by simplifying these equations via boundary-layer approximation. The standard procedure to this approximation is first to rewrite the governing equations in a stretched coordinate system by letting

$$x=Lx^* \tag{15}$$

$$y=Ly^*/(R_{e,\rho})^{\frac{1}{n+1}} \tag{16}$$

$$u=U_o u^* \tag{17}$$

$$v=U_o v^*/(R_{e,\rho})^{\frac{1}{n+1}} \tag{18}$$

$$p=\rho U_o^2 p^* \tag{19}$$

$$U_e=U_o U_e^* \tag{20}$$

$$T^*=(T_w-T)/(T_w-T_e) \tag{21}$$

$$C^*=(C_w-C)/(C_w-C_e) \tag{22}$$

In the above, $R_{e,\rho}=U_o^{2-n}L^n\rho/m$ is the generalized Reynolds number [6]. The governing equations in terms of dimensionless variables read

$$\frac{\partial u^*}{\partial x^*}+\frac{\partial v^*}{\partial y^*}=0 \tag{23}$$

$$u^*\frac{\partial u^*}{\partial x^*}+v^*\frac{\partial u^*}{\partial y^*}=U_e^*\frac{\partial U_e^*}{\partial x^*}+\frac{\partial}{\partial y^*}\left(\frac{\partial u^*}{\partial y^*}\right)^n \tag{24}$$

$$\frac{\partial p^*}{\partial y^*}=0 \tag{25}$$

$$u^*\frac{\partial T^*}{\partial x^*}+v^*\frac{\partial T^*}{\partial y^*}=\frac{1}{P_{r,\rho}}\frac{\partial^2 T^*}{\partial y^{*2}} \tag{26}$$

$$u^*\frac{\partial C^*}{\partial x^*}+v^*\frac{\partial C^*}{\partial y^*}=\frac{1}{S_{c,\rho}}\frac{\partial^2 C^*}{\partial y^{*2}} \tag{27}$$

In the above eqs. $P_{r,\rho}$ and $S_{c,\rho}$ are respectively generalized Prandtl number and generalized Schmidt number defined by

$$P_{r,\rho}=\frac{C_p\rho LU_o}{k\,R_{e,\rho}^{\frac{2}{n+1}}}=P_r\frac{R_e}{R_{e,\rho}^{\frac{2}{n+1}}} \tag{28}$$

$$S_{c,\rho}=\frac{L\,U_o}{R_{e,\rho}^{\frac{2}{n+1}}}=S_c\frac{R_e}{R_{e,\rho}^{\frac{2}{n+1}}}\ , \tag{29}$$

where R_e, P_r and S_c are Reynolds, Prandtl, and Schmidt numbers, respectively. On going from eqs. (1)-(5) to (23)-(27), boundary-layer approximation has been introduced, i.e., terms divided by $(R_{e,\rho})^{\frac{1}{n+1}}$ has been dropped. The second momentum eq. (eq.25) simply dictates that there is no significant pressure variation across the boundary layer even for power-law fluids. This presumes high Reynolds number but should be valid for all kinds of fluids that may be approximated by power-law constitutive equation.

Boundary conditions corresponding to eqs.(23)-(27) are

$$u^*(x^*,0)=v^*(x^*,0)=0 \tag{30}$$

$$u^*(x^*,\infty)=U_e^* \tag{31}$$

$$T^*(x^*,0)=0 \tag{32}$$

$$T^*(x^*,\infty)=1 \tag{33}$$

$$C^*(x^*,0)=0 \tag{34}$$

$$C^*(x^*,\infty)=1 \tag{35}$$

3. Similarity-type transformation

Boundary-layer calculation has conventionally been performed in similarity-type variable domain. The one introduced here is Göetler-type variables which have been proved very useful for a laminar boundary-layer calculation [7-10].

$$\xi=\int_0^{x^*}U_e^*dx^* \tag{36}$$

$$\eta=U_e^*y^*/\sqrt{2\xi} \tag{37}$$

A normalized streamwise velocity and a modified normal velocity are now introduced according to

$$F=u^*/U_e^* \tag{38}$$

$$V=2\xi\frac{\partial\eta}{\partial x^*}\frac{F}{U_e^*}+\frac{\sqrt{2\xi}}{U_e^*}v^* \tag{39}$$

In terms of new independent variables and dependent variables defined above, the boundary-layer equations read

$$2\xi\frac{\partial F}{\partial\xi}+F+\frac{\partial V}{\partial\eta}=0 \tag{40}$$

$$a_0\frac{\partial^2F}{\partial\eta^2}+a_1\frac{\partial F}{\partial\eta}+a_2F+a_3+a_4\frac{\partial F}{\partial\xi}=0 \tag{41}$$

$$\frac{\partial^2T^*}{\partial\eta^2}+b_1\frac{\partial T^*}{\partial\eta}+b_2T^*+b_3+b_4\frac{\partial T^*}{\partial\xi}=0 \tag{42}$$

$$\frac{\partial^2C^*}{\partial\eta^2}+c_1\frac{\partial C^*}{\partial\eta}+c_2C^*+c_3+c_4\frac{\partial C^*}{\partial\xi}=0, \tag{43}$$

where the variable coefficients are

$$a_0=n \tag{44}$$

$$a_1=-V \tag{45}$$

$$a_2=-\beta F,\ \beta=\frac{2\xi}{U_e^*}\frac{\partial U_e^*}{\partial\xi} \tag{46}$$

$$a_3=\beta \tag{47}$$

$$a_4=-2\xi F \tag{48}$$

$$b_1=a_1P_{r,\rho} \tag{49}$$

$$b_2=b_3=0 \tag{50}$$

$$b_4=a_4P_{r,\rho} \tag{51}$$

$$c_1=a_1S_{c,\rho} \tag{52}$$

$$c_2=c_3=0 \tag{53}$$

$$c_4=a_4S_{c,\rho} \tag{54}$$

The above governing equations have been numerically integrated using a finite difference method. An equal spacing, i.e., $\Delta\xi=0.005$ or 0.01 has been provided in streamwise direction. However, a variable grid spacing has been used for η derivatives. The one adopted here is based on the geometric progression;

$$\Delta\eta_i=(\varkappa)^{i-1}\Delta\eta_1 \qquad i=1,2,\cdots\cdots \tag{55}$$

In the above, $\Delta\eta_1$ is the spacing between the second grid point and the wall. This particular approach has been found to be satisfactory by a number of investigators [11]. The total thickness of the η-strip is given by

$$\eta_{\bar m}=\Delta\eta_1\left(\frac{1-\varkappa^{\bar m-1}}{1-\varkappa}\right)\ \varkappa\neq1 \tag{56}$$

where m denotes the total number of grid points across the η-strip. For given $\eta_{\bar m}$, $\varkappa$ and $\bar m$ the spacing of the grid points is then well defined. For each particular problem the optimum values of $\Delta\eta_1$, $\varkappa$ and $\bar m$ are selected. For the present problem, $\Delta\eta_1=0.004$, $\varkappa=1.08$ and $\bar m=81$ were found to be practical.

The numerical integration proceeded in an implicit manner in the direction of increasing ξ. At each stage of ξ, eqs. (40) and (41) were first solved for V and F following Carnahan et al. [12], and the results were fed to eq. (42) to obtain temperature profile. The computation time for power-law boundary-layer code exceeded by 20-30% compared to that of Newtonian due to the nonlinearity in constitutive equation.

Boundary-layer flow is driven by the outer flow, an important flow characteristic such as turbulence level and blockage effect. The outer flow equation for a 2-D symmetric body should include a leading linear term to guarantee a stagnation point, and terms of odd order

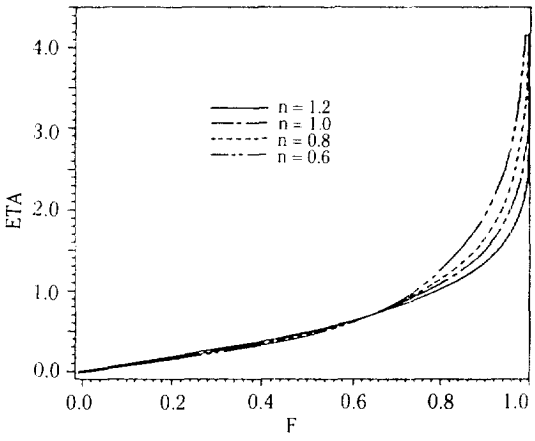

Fig. 2. Boundary-layer velocity distributions of power-law materials at $\theta = 20$ degrees.

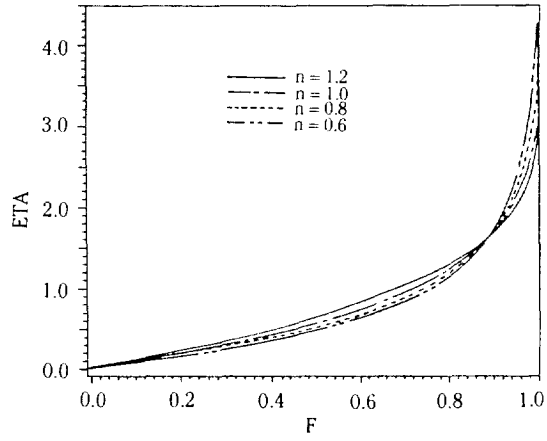

Fig. 3. Boundary-layer velocity distributions of power-law materials at $\theta = 60$ degrees.

only to ensure the symmetry of the flow. Though classical, a most reliable outer flow equation is Hiemenz outer flow distribution. This is a polynominal fitted to the experimental data [2] given by the formula

$$U_e^* = 1.814\,x^* + 0.271\,x^{*3} + 0.047\,x^{*5} \qquad (57)$$

RESULTS AND DISCUSSION

Present numerical solution for the boundary-layer flows of power-law fluid may be considered exact. There was no limitations on the generalized Prandtl number and flow behavior index. Therefore, any anomalous transport behavior of different power-law fluids are entirely due to the different characteristics of the non-Newtonian materials. There was no additional difficulty in running the power-law program over the Newtonian case.

The boundary-layer velocity profiles at $\theta = 20°$ and 60° are shown in Figs. 2 and 3. The viscous velocity of pseudoplastic materials is larger near the wall and smaller near the freestream compared to Newtonian fluid. It is also clear that as the fluid is more shear thinning (smaller n) the above tendency is exaggerated. Exactly the opposite is true for the dilatant material, i.e., the velocity profile for dilatant material is smaller near the wall and larger near the edge compared to Newtonian fluid. The same tendency was also reported for flows over flat plate [1]. This anomaly may easily be understood when the shear rate distribution across the boundary-layer is considered. In boundary-layer flow, shear rate is maximum near the wall and minimum near the edge where it tends to zero. Therefore, as the material becomes more shear thinning, a smaller viscosity and larger velocity is dictated near the wall, and a larger viscosity and smaller velocity is obtained near the edge. Exactly the opposite can be applied for dilatant materials.

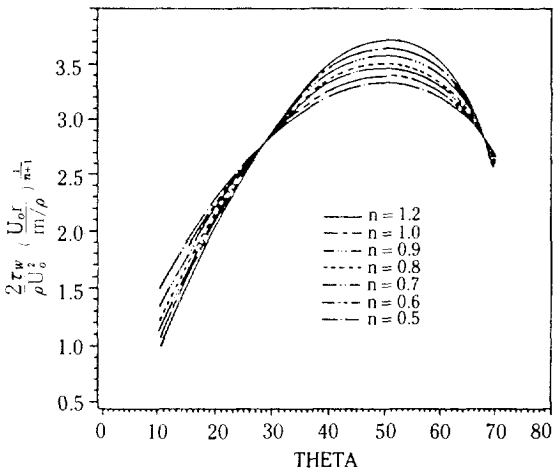

Fig. 4. Skin friction of power-law materials predicted with Himenz' outer flow equation.

The skin friction around a circular cylinder in crossflow is maximum at about $\theta = 50$-60° depending on flow conditions, and tends to vanish as the point of separation nears for Newtonian fluid [13,14]. The point of separation is actually oscillating due to the natural shedding. Following Dwyer and McCroskey[13], the time-averaged point of separation from surface oil flow experiment is $78 \pm 1°$ for laminar flows. In numerical calculation, the predicted point of separation is very sensitive to the outer flow equation. The point of separation calculated from the present boundary-layer code using Hiemenz outer flow equation was approximately 79.5°.

Presently calculated skin friction for power-law

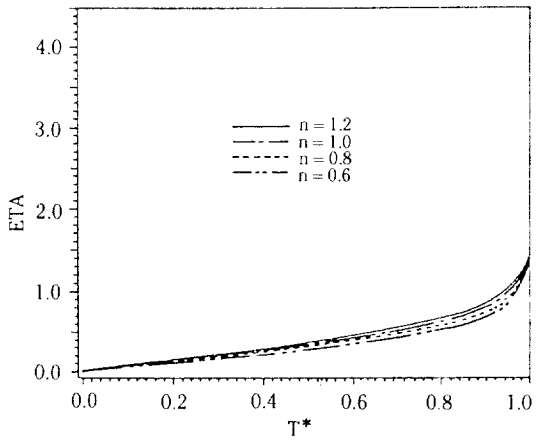

Fig. 5. Boundary-layer temperature distributions of power-law materials at θ= 20 degrees.

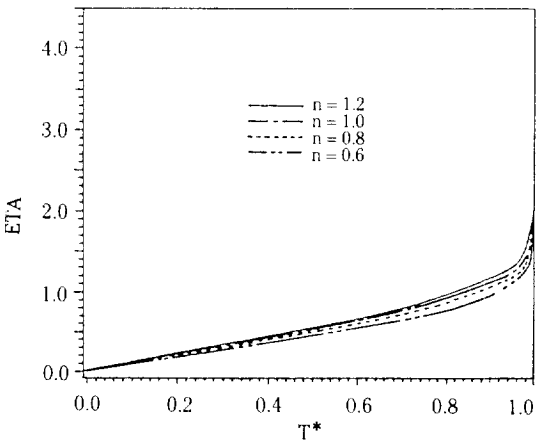

Fig. 6. Boundary-layer temperature distributions of power-law materials at θ= 60 degrees.

fluids is given in Fig. 4. Up to approximately θ=30° from the front stagnation point, the skin friction increases as the value of n decreases. Beyond this, the tendency is reversed, and a second cross is noticed at around θ = 65°. As far as the boundary-layer flow is established, wall properties should follow Newtonian in nature. For Newtonian, skin friction i.e., wall shear rate increases up to about θ = 50-60°, as mentioned above and as shown in the figure. Therefore, up to approximately this point, the power-law viscosity decreases for n<1, and increases for n>1, and the tendency in Fig. 4 is expected.

Temperature distribution and therefore heat transfer is not directly related to the non-Newtonian viscosity, but uniquely determined by the velocity distribution as far as the fluid is purely viscous and under forced convection. The connection between temperature distribution and non-Newtonian viscosity comes into play only through the velocity field.

With $P_{r,p}$ = 14, boundary-layer temperature distributions at θ= 20°, and 60° are shown in Figs. 5 and 6, respectively. The growth of thermal boundary-layer along downstream, and its much thinner thickness compared to that of velocity boundary-layer are obvious. More importantly, temperature profile becomes larger as the value of n decreases and this is not reversed, unlike the velocity profile, as one moves away from the surface. This however may be easily understood by taking a further look at the corresponding velocity profiles (Figs. 2 and 3). Near the wall, the viscous velocity becomes larger as the value of n decreases, and the thermal boundary-layer is mostly confined to this region of velocity field. With a larger velocity profile, a larger temperature profile results under fored convection.

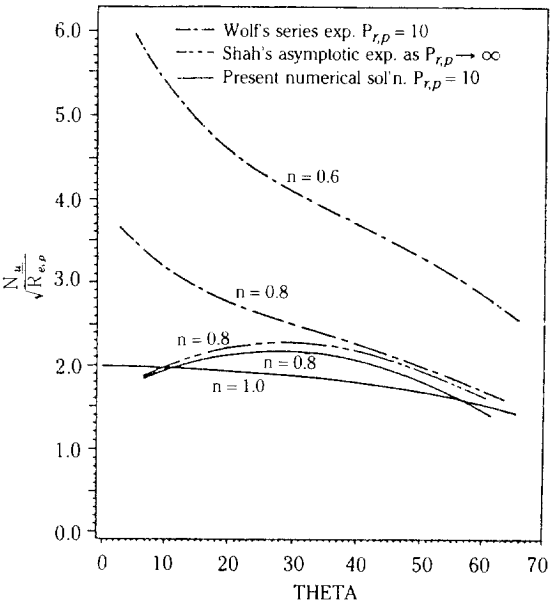

Fig. 7. Local rate of heat transfer for pseudoplastic materials.

Shown in Fig. 7 is the presently calculated heat transfer for n = 0.8 and $P_{r,p}$ = 10. Also shown in the same figure are analytical approximation by other investigators. The predicted heat transfer shows a considerable deviation between them. Aside from the present numerical solution for n = 0.8, pedictions by two others show a contradiction even in tendency. Present result using the outer flow equation by Shah et al. is similar to that of Shah et al. [3], however with a lower value of predicted heat transfer for the present case. This perhaps is from the lower value of $P_{r,p}$ = 10

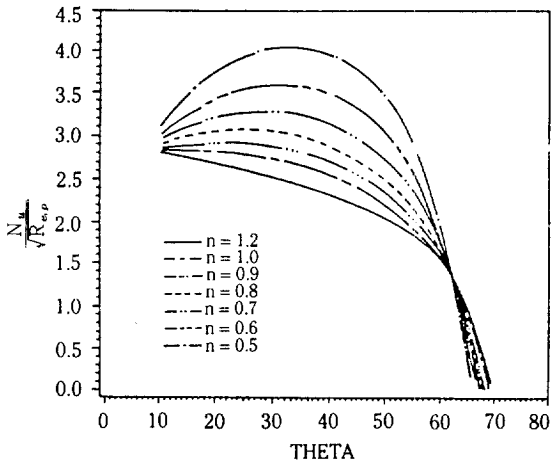

Fig. 8. Heat transfer of power-law materials predicted with Hiemenz' outer flow equation.

employed presently, compared to ∞ by Shah et al.. With a very large value of $P_{r,p}$, the thermal boundary-layer is very thin, the velocity profile covering the thermal boundary-layer is presumably linear. Following Shah et al., their prediction was in good agreement with the experimental data.

Two crossover points between n = 0.8 and n = 1.0 are also noted from Fig. 7. This probably is due to the skin friction distribution given in Fig. 4. The skin friction, i.e., the wall shear rate is maximum at about θ = 50-60°, and becomes zero at the front stagnation point and at the point of separation as well. For n < 1, higher rate of shear gives a lower viscosity and larger velocity and temperature leading to a increased heat transfer. At zero or low rate of shear, i.e., near the two characteristic points, the viscosity for n = 0.8 would be larger than that of Newtonian and this gives smaller velocity and temperature leading to a decreased heat transfer for pseudoplastic materials. Therefore two crossover points in Fig. 7 are expected.

Presently calculated heat transfer for a wide range of flow behavior index with $P_{r,p}$ = 14 is given in Fig. 8. For the major portion of the attached flow, the rate of heat transfer increases as the value of n decreases. Heat transfer of pseudoplastic is higher than that of Newtonian which, on the other hand, is higher compared to that of dilatant. However, as one nears front stagnation point or point of separation, the tendency is reversed. Identically the same tendency was true for skin friction. This is not unexpected at all. Under forced convection heat transfer is essentially governed by velocity field, and this viscous velocity is again determined from the shear dependent viscosity for power-law materials. With a larger streamwise velocity near the wall for a more shear-thinning material, a higher velocity and temperature gradients are dictated resulting in a larger skin friction and heat transfer at wall.

CONCLUSION

Boundary-layer analysis of momentum, heat and mass transfer for power-law non-Newtonian fluids has been performed using a finite difference technique. Results obtained indicated that the heat transfer across the boundary-layer as well as the skin friction distribution is entirely governed by the flow behavior index(n) of power-law fluids via the boundary-layer velocity distribution.

NOMENCLATUE

C : concentration, kg mol/m^3
C_p : specific heat at constant pressure, J/kg°K
D : binary diffusivity, m^2/sec
k : consistency index, kg^{n-2}/m
L : radius of cylinder, m
n : flow behavior index
p : pressure, N/m^2
T : temperature, °K
u : streamwise velocity, m/s
v : normal velocity, m/s
x : streamwise coordinate, m
y : normal coordinate, m

Subscripts

e : condition at boundary-layer edge
o : condition in freestream
w : condition on the wall

Superscript

* : dimensionless variables in eqs. 15-22

Dimensionless Groups

N_u : local Nusselt number = hL/k (h = heat transfer coefficient, L = diameter of cylinder, k = thermal conductivity)
P_r : Prandtl number = $C_p\mu/k$
$P_{r,p}$: generalized Prandtl number defined by eq. (28)
R_e : Reynolds number = DU_o/ν
$R_{e,p}$: generalized Reynolds number
S_c : Schmidt number = ν/D
$S_{c,p}$: generalized Schmidt number defined by eq. (29)

Greek Letters

α : thern al diffusivity
η : normal coordinate defined by eq. (37)
μ : viscosity
ν : kinematic viscosity
ξ : streamwise coordinate defined by eq. (36)
ρ : density
τ : shear stress, N/m^2
θ : circumferential angle, deg

REFERENCES

1. Acrivos, A., Shah, M.I., and Petersen, E.E.: *AIChE J.*, **6,** 312 (1960).
2. Acrivos, A., Shah, M.I., and Petersen, E.E.: *AIChE J.*, **20,** 101 (1965).
3. Shah, M., Petersen, E., and Acrivos, A.: *AIChE J.*, **8,** 542 (1962).
4. Bizzel, G. and Slattery, J.: *Chem. Eng. Sci.*, **17,** 177 (1962).
5. Wlof, C. and Szewczyk, A.: 3rd Int'l Heat Trans.Conf. Chicago, 1966 Paper#37.
6. Takahashi, K.: 6th Int'l Heat Trans. Conf. New York, **5,** 335 (1979).
7. Kim, B.K.: Ph. D. Dissertation, Virginia Polytechnic Institute and State Univ., Blackage Virginia, 1985.
8. Kim, B.K., Borell, G., Cramer, M.S., Diller, T., and Telionis, D.P.: Proc. Symp. on Nonlinear Problems in Energy Eng., DOE CONF 830313, 96 (1983).
9. Kim, B.K., VanDenbrink, D., Cramer, M.S., and Telionis, D.P.: *AIChE J.*, **33,** 19 (1987).
10. Telionis, D.P.: "Unsteady Viscous Flow", Spring-Verlag, New York (1981).
11. Phillips, J.H.: *J. Appl. Mech.*, **58,** 561 (1973).
12. Carnahan, B., Luther, A.H., and Wilkers, J.O.: "Applied Numerical Methods", Wiley, 1969.
13. Dwyer, H.A. and McCroskey, W.J.: *J. Fluid Mech.*, **61,** 753 (1973).
14. Schlichting, H.: "Boundary-Layer Theory", 7th ed., McGraw Hill, New York (1979).